

Hadronization and Strangeness Production in a Chirally Symmetric Nonequilibrium Model

P. Rehberg and J. Aichelin

SUBATECH

*Laboratoire de Physique Subatomique et des Technologies Associées
UMR Université de Nantes, IN2P3/CNRS, Ecole des Mines de Nantes
4 Rue Alfred Kastler, F-44070 Nantes Cedex 3, France*

Abstract

The expansion and hadronization of a quark meson plasma is studied using an effective chiral interaction Lagrangian. The particles we consider are light as well as strange quarks, which can form pions, kaons and η mesons via collision processes. The transport equations for the system are solved using a QMD type algorithm. We find that in chemical equilibrium at high temperatures the strange quark mass is considerably higher than the strange current quark mass and becomes even higher if we assume an initial state free of strange quarks. This leads to a considerably higher production threshold. In contrast to simpler scenarios, like thermodynamics of free quarks with their bare mass, we observe that strangeness production in a plasma is hindered and not favoured. The different particle species created during the evolution become separated in coordinate as well as in momentum space. We observe, as at CERN experiments, a larger mean momentum of kaons as compared to pions. Thus the radial collective velocity may as well originate from a plasma expansion and not necessarily from a hadronic scenario.

PACS numbers: 12.38.Mh, 12.39.Fe, 24.10.Lx, 25.75.-q

Typeset using REVTeX

I. INTRODUCTION

The production of strange particles in relativistic heavy ion collisions has received lots of attention since it was proposed that their enhanced production could serve as an experimental signal for the creation of a quark-gluon plasma (QGP) [1]. In fact, it has been observed in sulfur-sulfur and lead-lead collisions at CERN that more strange particles have been produced than expected from an extrapolation of proton-proton or proton-nucleus collisions. Presently all cascade or string models fail to explain this enhancement in a hadronic scenario. Purely phenomenological models predict in addition that the disintegration of the plasma leads to the distillation of strangeness or to the formation of strangelets, i. e. droplets of multistrange quark matter which are stable for a sufficiently long time to be detected. Several experiments at Brookhaven and CERN are devoted to the search of such strangelets.

Therefore it is tempting to see whether approaches more closely related to quantum chromodynamics (QCD) can confirm strangeness enhancement if during the heavy ion collision a quark gluon plasma is formed. One of the major drawbacks in the interpretation of the experimental data is the lack of a theoretical model which is able to describe the formation, hadronization and decay of a QGP. An ideal model for a heavy ion collision should in principle be able to describe both quark and hadronic matter as well as the transition between these two regimes. Due to the expected short lifetime of a QGP, it should further be able to handle nonequilibrium effects. A theory accomplishing all of this is, however, unavailable nowadays, since the mechanisms leading to confinement are presently not understood. Although QCD is known via lattice calculations to contain this effect, a phenomenologically useful solution of this theory does up to now not exist, so that it is impossible to apply QCD to all stages of a heavy ion collision. This inhibits the construction of a theory which is able to explain all phenomena. It is nevertheless possible to construct nonequilibrium scenarios for effective interactions, which describe at least a part of the observed phenomena.

Especially for the low energy sector of strong interactions, it has been known for a long time that confinement does not play an important role. This sector is rather governed by chiral symmetry. One of the many effective chiral interaction Lagrangians known is the Nambu-Jona-Lasinio (NJL) model [2,3], which starts from

a Lagrangian containing quarks interacting via a four point coupling. This interaction leads to a spontaneous breakdown of chiral symmetry and to the appearance of light pseudoscalar mesons, which are bound states of quark-antiquark pairs. In the vacuum, it has been successfully applied to the computation of static quantities like hadronic mass spectra [3,4] or dynamic quantities like pion scattering lengths [5], to give only two examples. In the medium, it has been demonstrated that chiral symmetry becomes restored at sufficiently high temperatures and/or chemical potentials. In this case, the effective quark masses drop down, whereas the mesons cease to be bound states and become unstable resonances [6]. This effect models, to a certain extent, the deconfinement transition of QCD. In fact it can be seen by comparing the NJL mass spectra with lattice computations, as have been shown in Ref. [7], that the NJL model provides at least a qualitatively correct picture of strong interactions even beyond the chiral phase transition. The drawbacks of this model, however, are that it is nonrenormalizable and does not confine, so that one has free quarks at all temperatures.

Beside these successful applications to the equilibrium theory of strong interactions, the NJL model has recently been developed further towards a nonequilibrium formalism [8–10]. First numerical calculations within this formalism have been reported in Refs. [9,11–13]. The advantages of this approach compared to other effective models are obvious: Since one has both quark and hadronic degrees of freedom, where the latter appear, as in QCD, as bound states, one is, at least in principle, able to model a transition from an initial state, which contains only quarks, to a hadronic state. Since the numerical calculations needed turn out to be rather time consuming, the simplicity of the NJL model is another pluspoint.

The numerical method for the solution of the transport equations employed here is an algorithm of the quantum molecular dynamics (QMD) type [14], which means that we parametrize the Wigner function as a sum over double gaussians and solve the equations of motion for the parameters. This method has been chosen previously in the NJL model in Refs. [12,13]. The present paper is a follow up of Ref. [13], where we studied the two flavor version of the NJL model. Here we extend this work in including a third quark flavor, which enables us to study the production mechanisms of strange particles. Several results obtained in the framework of this model, which are not specific to three flavor calculations, have been reported in [13]

and will not be repeated here.

One of the major results we find here is that chiral symmetry predicts a much higher effective strange quark mass than the current mass of ca. 150 MeV. While this is the case already in equilibrium, where we find a strange quark mass of 300 MeV at a temperature of 350 MeV, the strange quark mass gets even further enhanced if one applies initial conditions which do not contain strange quarks. This raises the question, if the original models for strangeness enhancement, which are based on an assumed mass drop of the strange quark down to the current mass, have not been too naive. Unfortunately, since this is a generic nonequilibrium effect, it is not possible to confirm it via lattice simulations.

This paper is organized as follows: In Sec. II, we briefly review the three flavor NJL model and describe our numerical algorithm. Numerical results are presented in Sec. III. Section IV contains our summary and conclusions.

II. DESCRIPTION OF THE MODEL AND THE ALGORITHM

A. The Model

The model we use throughout this paper is the Nambu–Jona-Lasinio (NJL) model [2] in its three flavor version. This model is defined by the Lagrangian

$$\begin{aligned} \mathcal{L} = & \sum_{f=u,d,s} \bar{\psi} (i \not{\partial} - m_{0f}) \psi + G \sum_{a=0}^8 \left[\left(\bar{\psi} \lambda_a \psi \right)^2 + \left(\bar{\psi} i \gamma_5 \lambda_a \psi \right)^2 \right] \\ & + K \left[\det \bar{\psi} (1 + \gamma_5) \psi + \det \bar{\psi} (1 - \gamma_5) \psi \right] \quad . \end{aligned} \quad (2.1)$$

Here, ψ denotes the quark fields, which are implicitly understood to carry flavor and color indices. The matrices λ_a are the Gell-Mann matrices in flavor space for $a = 1, \dots, 8$ and $\lambda_0 = \sqrt{2/3} \mathbf{1}$. A small explicit chiral symmetry breaking is provided by the current quark masses m_{0f} . G and K are coupling constants with dimensions MeV^{-2} and MeV^{-5} , respectively. The 't Hooft determinant proportional to K serves to model the $U_A(1)$ symmetry breaking, which in QCD takes place by an effective interaction of $2N_f$ quarks due to instanton effects.

The properties of the Lagrangian (2.1) have been extensively studied in the literature. We thus review here only briefly those topics of the NJL model, which are essential for the understanding of the present article and refer for more details to

Ref. [3]. The most important feature of the interaction (2.1) is that it preserves the chiral symmetry of QCD, i.e. in the limit $m_{0f} \rightarrow 0$ it is invariant under transformations of the form

$$\psi \rightarrow \exp \left(-i\gamma_5 \sum_{a=1}^8 \theta_a \lambda_a \right) \psi \quad (2.2)$$

for arbitrary real θ_a . In the vacuum, this symmetry is spontaneously broken and the quarks obtain an effective mass. As a consequence of the Goldstone theorem, eight massless modes appear as bound states in the quark-antiquark scattering matrix. These massless modes carry the quantum numbers of the light pseudoscalar mesons, i.e. one obtains three pions, four kaons and one η meson. The η' meson, which appears also as a pole in the quark-antiquark scattering matrix, is massive due to the $U_A(1)$ breaking by the 't Hooft determinant. For finite current quark masses, $m_{0f} \neq 0$, this picture changes slightly in that chiral symmetry is no longer an exact symmetry. This leads to finite meson masses, which, by parameter choice, can be adjusted to the experimentally observed values.

At sufficiently large temperatures and/or chemical potentials, chiral symmetry becomes restored. This means that in this region of the phase diagram the quark mass is either zero for $m_{0f} = 0$ or at least low for $m_{0f} \neq 0$. The mesons, on the other hand, are no longer bound states but become resonant states, which have a finite width due to the possible decay channel $M \rightarrow q\bar{q}$.

To give a quantitative picture, we show in Fig. 1 the masses of the constituent quarks at chemical potential $\mu = 0$ as a function of the temperature. In this figure, the masses are computed using the Hartree approximation, which is the leading order of an expansion in the inverse number of colors, $1/N_c$ [15]. This leads to the gap equation

$$m_i = m_{0i} - \frac{GN_c}{\pi^2} m_i A_i + \frac{KN_c^2}{8\pi^4} m_j A_j m_k A_k \quad , \quad i \neq j \neq k \neq i \quad (2.3a)$$

$$A_i = -8\pi^2 \int_{|\vec{p}| < \Lambda} \frac{d^3p}{(2\pi)^3} \frac{1}{\sqrt{\vec{p}^2 + m_i^2}} \left(1 - \frac{n_i + n_{\bar{i}}}{2N_c} \right) \quad , \quad (2.3b)$$

where the indices i, j and k run over all three quark flavors. The phase space distribution of quarks and antiquarks of flavor i is denoted by n_i and $n_{\bar{i}}$, respectively. In equilibrium, they are given by the Fermi distribution function. Since the NJL model is nonrenormalizable, the integral in Eq. (2.3b) has been limited to momenta

smaller than an $O(3)$ cutoff Λ . The parameters used in Fig. 1 are $m_{0q} = 5.5$ MeV, $m_{0s} = 140.7$ MeV, $G\Lambda^2 = 1.835$, $K\Lambda^5 = 12.36$ and $\Lambda = 602.3$ MeV, where we use the generic index q to denote both u and d . At $T = 0$, chiral symmetry is spontaneously broken and one obtains constituent quark masses of $m_q = 368$ MeV and $m_s = 550$ MeV. These masses stay more or less constant up to a temperature of approximately 200 MeV, where the light quark mass drops down to a value close its bare value. The strange quark mass, on the other hand, also drops down but stays relatively large. At $T = 350$ MeV, which is far beyond any temperature to be expected in a heavy ion experiment, one still has an effective strange quark mass of $m_s = 300$ MeV, which is about two times the bare strange quark mass.

Mesons appear as poles in the quark-antiquark scattering matrix. A computation of this quantity leads to the meson dispersion relation [3]

$$1 - 2G\Pi_{PS}^R(p) = 0 \quad , \quad (2.4)$$

where $\Pi_{PS}^R(p)$ is the irreducible retarded pseudoscalar polarization function. In lowest order of $1/N_c$ it is given by the diagram shown in Fig. 2. The temperature dependence of the meson masses is shown in Fig. 3, together with the temperature dependence of $2m_q$ and $m_q + m_s$. The pion mass is denoted by the solid line of Fig. 3. At zero temperature, its mass is equal to the experimental value of 135 MeV. This mass stays roughly constant until it begins to rise at a temperature around 200 MeV. At the pion Mott temperature $T_{M_\pi} = 212$ MeV, which is marked by the arrow in Fig. 3, its mass becomes equal to that of its constituents, $m_\pi(T_{M_\pi}) = 2m_q(T_{M_\pi})$, and stays above at higher temperatures. In this temperature range, the pion becomes unstable due to a Mott effect and obtains a finite width corresponding to the decay channel $\pi \rightarrow q\bar{q}$. This Mott effect models to a certain extent the deconfinement transition of QCD. For more details about the Mott transition in the NJL model see Ref. [6].

The kaon behaves in a similar way. At zero temperature, one obtains a mass of 497 MeV. At the kaon Mott temperature T_{M_K} one has $m_K(T_{M_K}) = m_q(T_{M_K}) + m_s(T_{M_K})$ and the kaon becomes unstable at higher temperatures. Numerically, one finds $T_{M_K} = 210$ MeV $\approx T_{M_\pi}$. The same behaviour is found for the η meson. Whereas one has $m_\eta = 515$ MeV at zero temperature, one finds a Mott transition at $T_{M_\eta} = 180$ MeV and an unstable resonance above. The η' is special, since due to its large mass and the lack of confinement in the NJL model it is unstable at all

temperatures. For this reason and because the hadronization cross sections for the η' production are comparatively low [16], we will not consider the η' further.

B. The Simulation Algorithm

Our simulation is based on the observation, that both quark and meson degrees of freedom can be described *simultaneously* by transport equations of the Boltzmann type [10],

$$\left(\partial_t + \vec{\partial}_p E \vec{\partial}_x - \vec{\partial}_x E \vec{\partial}_p\right) n(\vec{x}, \vec{p}, t) = I_{\text{coll}}[n(\vec{x}, \vec{p}, t)] \quad (2.5)$$

where $n(\vec{x}, \vec{p}, t)$ is the Wigner function of the particle species in question and E the corresponding quasiparticle energy. This quantity is in general a complicated function of \vec{x} , \vec{p} and t , which has to be determined in a selfconsistent fashion from a diagrammatic expansion of the self energy or the irreducible polarization, respectively [10]. In the following, we will make the approximation

$$E(\vec{x}, \vec{p}, t) = \sqrt{\vec{p}^2 + m(\vec{x}, t)^2} \quad , \quad (2.6)$$

where the quasiparticle mass $m(\vec{x}, t)$ is determined either from Eq. (2.3) for quarks or from the solution of Eq. (2.4) with $\vec{p} = 0$ for mesons.

For the solution of Eq. (2.5) we employ an algorithm of the QMD type [14]. To this end, we parametrize the Wigner function as a sum over double Gaussians,

$$n(\vec{x}, \vec{p}, t) = \sum_{i=1}^N \exp\left(-\frac{(\vec{r} - \vec{r}_i(t))^2}{2w^2}\right) \exp\left(-\frac{w^2}{2}(\vec{p} - \vec{p}_i(t))^2\right) \quad . \quad (2.7)$$

The normalization is chosen in such a way that the integral over n is equal to the total number of particles,

$$\int \frac{d^3x d^3p}{(2\pi)^3} n(\vec{x}, \vec{p}, t) = N \quad . \quad (2.8)$$

The centroids $r_i(t)$, $p_i(t)$ move along the characteristics of Eq. (2.5), i. e.

$$\dot{\vec{x}}_i(t) = \vec{\partial}_p E(\vec{x}_i(t), \vec{p}_i(t), t) \quad (2.9a)$$

$$\dot{\vec{p}}_i(t) = -\vec{\partial}_x E(\vec{x}_i(t), \vec{p}_i(t), t) + \text{collision contributions} \quad . \quad (2.9b)$$

The collision processes which enter in Eq. (2.9b) belong to three different classes:

(i) quark elastic scattering processes, $qq \leftrightarrow qq$, $q\bar{q} \leftrightarrow q\bar{q}$ and $\bar{q}\bar{q} \leftrightarrow \bar{q}\bar{q}$ [17], (ii)

hadronization processes, $q\bar{q} \leftrightarrow MM$ [16,18] and (iii) meson decay processes $M \rightarrow q\bar{q}$ [10]. The first of these two classes are treated in the following fashion: For each particle pair, we perform a transformation to the rest system of the pair and check, whether these two particles will have their closest approach within the current time step, which is a necessary condition for a collision to happen. If this condition is fulfilled, we compute the cross sections σ_k for each process, which is possible for the incoming pair, and the total cross section $\sigma_{\text{tot}} = \sum \sigma_k$. A collision happens if the minimal distance of the particle trajectories is smaller than $\sqrt{\sigma_{\text{tot}}/\pi}$. The actual collision process is chosen randomly with probability $\sigma_k/\sigma_{\text{tot}}$. Neglecting anisotropies of the differential cross section, we choose the scattering angle randomly in the rest frame of the collision. This scheme works if one has a scattering process with two particles in the initial state. For the meson decay processes, which are only possible in the early stage of the expansion, when mesons exist as resonances, we proceed by computing the mean life time τ of the meson in question and decide with probability $1 - \exp(-\Delta t/\tau)$, where Δt is the time step, whether the meson decays during this iteration or not. If the decay takes place, we again choose the momenta of the outgoing quarks randomly in the particle rest frame and boost them to the original frame.

The numerical task to accomplish consists thus in a numerical solution of Eq. (2.9) together with Eqs. (2.3), (2.4), where the particle distribution functions appearing in the two latter equations have to be replaced by the parametrization (2.7). For the computation of the collision contributions, one has also to compute cross sections, which themselves are complicated functionals of the particle distribution functions [16–18]. Doing this exactly is a task which lies far beyond present days computer capacities. We thus decide to take a shortcut in defining effective thermal quantities. This works as follows: at each time step, we solve Eq. (2.3) with Eq. (2.7) inserted for the quark masses. Afterwards, we define an effective temperature with the help of the equation

$$m_q(\vec{x}, t) = m_q^{\text{eq}}(T_{\text{eff}}(\vec{x}, t)) \quad , \quad (2.10)$$

where $m_q^{\text{eq}}(T)$ is the equilibrium temperature dependence of the light quark mass. The meson masses are then computed from the equilibrium expressions, which are functions of T_{eff} , m_q and m_s . Mass gradients, which enter Eq. (2.9b), are computed via an exact differentiation of Eq. (2.3) for quarks, whereas for mesons we take

$$\vec{\partial}_x m_M = \left[\frac{\partial m_M^{\text{eq}}}{\partial T} \left(\frac{dm_q^{\text{eq}}}{dT} \right)^{-1} + \frac{\partial m_M^{\text{eq}}}{\partial m_q} \right] \vec{\partial}_x m_q + \frac{\partial m_M^{\text{eq}}}{\partial m_s} \vec{\partial}_x m_s \quad (2.11)$$

in agreement with our prescription for the computation of the meson masses. At last we compute the scattering cross sections as functions of T_{eff} as well as the quark and meson masses, again using equilibrium expressions. Note that this procedure does not necessarily give the same numbers as in thermal equilibrium, since we have *two* independent parameters, m_q and m_s , which in thermal equilibrium are coupled to each other, whereas there is no unique relation between these two quantities in our nonequilibrium calculation. Since we do not consider baryons in our hadronization processes, we limit ourselves to systems with zero baryon density, i. e. we set $\mu_q = \mu_s = 0$ in all equilibrium expressions.

As initial condition we use a spherically symmetric system with a given radius r_0 , in which the spatial centroids of the quark distribution functions are distributed with uniform probability. For the momentum centroids of the light quark distribution function, we choose a Fermi distribution,

$$P(\vec{p}) \sim \frac{2N_c}{\exp\left(\sqrt{\vec{p}^2 + m_q^{\text{eq}}(T_0)^2}/T_0\right) + 1} \Theta(\Lambda - p) \quad . \quad (2.12)$$

In this distribution, T_0 is a free parameter. The number of light quarks per flavor and particle/antiparticle degree of freedom is fixed as the momentum integral over the Fermi distribution (2.12) times the volume. The Θ -factor serves to cut off the distribution function at momenta larger than Λ . This is necessary, since due to the cutoff in Eq. (2.3) energy conservation is only valid strictly if no particles with momenta larger than Λ are present in the system [9]. We nevertheless expect this effect not to be of great importance, so that below we will also study initial conditions without this factor. For the strange quarks, the momentum distribution is chosen to be

$$P(\vec{p}) \sim f_s \frac{2N_c}{\exp\left(\sqrt{\vec{p}^2 + m_s^{\text{eq}}(T_0)^2}/T_0\right) + 1} \Theta(\Lambda - p) \quad . \quad (2.13)$$

This differs from Eq. (2.12) by the factor f_s , which serves to adjust the degree of chemical equilibration in the initial state. For $f_s = 0$, one has no strangeness at all initially, whereas for $f_s = 1$ one starts with a totally equilibrated system.

III. NUMERICAL RESULTS

In this section we present the numerical outcome of our calculations. The NJL parameters we use throughout this section are $m_{0q} = 5.5 \text{ MeV}$, $m_{0s} = 140.7 \text{ MeV}$, $G\Lambda^2 = 1.835$, $K\Lambda^5 = 12.36$ and $\Lambda = 602.3 \text{ MeV}$. The width of the wave packets was chosen to be 2 fm . The initialization temperature in Eqs. (2.12), (2.13) was taken to be $T_0 = 280 \text{ MeV}$.

A. Space-Time Dependence of Quark Masses

The evolution of the space-time dependence of the constituent quark masses can be seen from Fig. 4. Here we show the constituent quark masses as a function of r for different times. In this calculation, no strange quarks were present in the initial state, but Eq. (2.3) involves nevertheless also the computation of the strange quark mass. At $t = 0$, the light quark mass is low in the center, where the particle density is high. It begins to rise near the surface due to the gaussian shape of the parametrization (2.7). Since our program computes the constituent quark masses only at those points, where particles are present, the plot stops at the maximal radius $r_0 = 7 \text{ fm}$. At later times, the particles flow out and thus the particle density drops. This leads to an increase of the light quark mass. At $t = 25 \text{ fm}/c$, one has everywhere a light quark mass equal to the vacuum mass. The strange quark mass behaves similar, but there is one important difference between strange and light quarks: Whereas the value of the light quark mass in the centre is low, as one would expect from a hot system, the strange quark mass is much higher as in the thermal case. Numerically, one has $m_q = 41 \text{ MeV}$ and $m_s = 464 \text{ MeV}$ in the centre, whereas for a thermal system one would have $m_q = 23 \text{ MeV}$ and $m_s = 353 \text{ MeV}$ at $T = 280 \text{ MeV}$. The discrepancy is not very large for the light quarks, but amounts to 110 MeV for the strange quarks. As will be seen below, this effect has a large impact on the production of strange particles, because the production threshold rises considerably. The reason for this effect can be seen from Eq. (2.3): writing this equation explicitly for light and strange quarks, one has

$$m_q = m_{0q} - \left(G - \frac{KN_c}{8\pi^2} m_s A_s \right) \frac{N_c}{\pi^2} m_q A_q \quad (3.1a)$$

$$m_s = m_{0s} - \frac{GN_c}{\pi^2} m_s A_s + \frac{KN_c^2}{8\pi^4} (m_q A_q)^2 \quad . \quad (3.1b)$$

Note that all selfenergy contributions on the right hand side of Eqs. (3.1) increase the mass and have their maximum at vanishing density. Since $n_s(\vec{x}, \vec{p}, t = 0) = 0$, the second term on the right hand side of Eq. (3.1b) does *not* receive direct medium corrections and thus gives a *larger* contribution to the mass as it would do in chemical equilibrium. There are medium corrections to the strange quark mass entering through the third term on the right hand side of Eq. (3.1b) which cause the mass drop in the centre, which is seen in Fig. 4. However, these contributions are not sufficient to generate a strange quark mass near the thermal strange quark mass. In order to have the strange quarks equilibrated, they first have to be created with a much larger mass than the equilibrium mass, which makes it difficult for the system to approach equilibrium.

We would like to stress that this effect can presently only be seen in phenomenological models like the NJL model. Since it is a nonequilibrium effect, there are no means to reproduce or to disprove it in lattice calculations.

B. Particle Multiplicities and Meson Production Mechanisms

A first account of the meson production mechanisms in the NJL model has been given in Ref. [13], where the expansion and hadronization of a two flavor plasma has been studied. The general results reported there remain true for a three flavor plasma. Nevertheless, there are some phenomena of a three flavor plasma, which do not exist in a two flavor plasma.

One of these aspects which can be studied within our hadronization model for a quark gluon plasma are the particle multiplicities, especially the ratio of strange to nonstrange particles. These quantities are interesting because it was claimed already several years ago that they could serve as an experimental signal for the creation of a quark-gluon plasma [1]. Due to the shortcomings of our model, we cannot expect to obtain precise numbers for the particle multiplicities, but we expect to obtain a qualitatively reasonable estimate. To this end, we show in Tab. I the multiplicities obtained from the initial conditions (2.12), (2.13) for different initial radii. It can be seen that for small r_0 the final state consists mostly of light quarks, whereas for larger systems the most abundant particle species are pions. This can be explained with the shorter lifetime of the smaller systems, which inhibits a complete conversion

of all quarks into mesons. As the system size becomes larger, the lifetime increases, thus allowing more quarks to create hadrons [13].

It can also be seen in Tab. I that the final state contains very few kaons and strange quarks; even in the largest system the ratio of strange particles to all particles is about 1%. The reason for this is the large strange quark mass together with the Θ -factor in Eqs. (2.12), (2.13). Due to the large strange quark mass, a pair of a light quark and antiquark must have a large kinetic energy in order to be able to create a strange-antistrange pair via the process $u\bar{u}, d\bar{d} \rightarrow s\bar{s}$. Due to cutoff in the initial conditions, on the other hand, such pairs do not occur very frequently. The same mechanism inhibits the creation of kaons from light quark pairs, since the kaon mass is of the same order of magnitude as the strange quark mass. Furthermore, the cross section for the creation of kaons from light quark pairs is small compared to the cross section for their creation from strange quarks, so that kaons are most efficiently produced from the latter [16]. One observes, on the other hand, a comparably large multiplicity of η mesons, which on a first glance might be surprising, since η mesons have about the same mass as kaons. A closer look at the production mechanisms shows however that η mesons are predominantly created by processes of the type $u\bar{u} \rightarrow \pi^0\eta$ and variations hereof. This leads to a smaller mass gap and thus to a larger η than kaon production. We conclude thus that it is easier to obtain a chemical equilibrium for η mesons than for kaons, which might be a fact which persists to more realistic models. Experimentally, this should be easy to verify once the absolute multiplicities are known, since the η has about the same mass as the kaon, so that the multiplicity ratio in equilibrium is given by the relative degrees of freedom: one has $N_\eta/N_K = 1/4$ in chemical equilibrium, $N_\eta/N_K > 1/4$ outside chemical equilibrium.

Since the multiplicity of strange particles cannot be reasonably discussed using initial conditions containing a momentum cutoff, we have also performed calculations with the Θ -factors in Eqs. (2.12) and (2.13) dropped. While this does not give a large effect on the particle masses, one has more high momentum quark pairs at hand to create also heavier particles. As already mentioned, this is paid with the loss of exact energy conservation [9], but we do not expect this effect to have a large impact. The result for the multiplicities is shown in Tab. II. As in Tab. I, it can be seen that the ratio of mesons to quarks rises with r_0 . The ratio of strange particles

to all particles stays approximately constant at a level of ca. 10%. The ratio N_η/N_K is always clearly above 1/4, thus indicating that a complete chemical equilibrium between these particles is not reached.

The evolution of the particle multiplicities with time for one of these runs with $r_0 = 6$ fm is shown in Fig. 5. It can be seen here that the production of mesons starts already at the beginning of the evolution. More details can be seen from Fig. 6, which shows the angular averaged particle density as a function of r for different times. As one can see here, the meson density is high at those points, where the quark density is high. Note however, that this is not true in the very early stage of the expansion, where the temperature in the centre is still high, as was discussed in Ref. [13].

As a third variant of the initial conditions, we display in Tab. III the particle multiplicities for the case that one has strange quarks in the initial state, i. e. $f_s = 1$ in Eq. (2.13). In this case, the ratio of strange particles to the total number of particles lies around 20%, which is consistent with the values obtained in heavy ion experiments [19]. The number of kaons is high compared to Tab. I, since now they can be produced efficiently from the strange quarks which are present in the initial state. In this case, the argument that an η meson can be produced more easily than a kaon remains no longer true, so that the ratio N_η/N_K is now lower than 1/4. Thus the N_η/N_K ratio may serve as a messenger of the strange quark content at the beginning of the expansion.

Comparing the multiplicities of Tabs. I–III, we find as a consequence that we can only obtain a strangeness ratio in the order of the experimentally observed one, if we assume that strange quarks are already present in the initial state. In an experimental situation, these might be created in collisions taking place before the plasma is formed, which we do not treat here.

The time dependence of the multiplicities for the calculation for $r_0 = 6$ fm of Tab. III is displayed in Fig. 7. The kaon production according to this figure proceeds fast in the beginning and terminates after 5 fm/ c . The pion production, on the other hand, has two components: one fast component until $t = 5$ fm/ c , followed by a slow rise at later times, which finally saturates. This time behaviour of the pion multiplicity is also found in calculations which do not contain strange quarks initially, although this is not shown explicitly here. The second component of the

pion production is, however, not observed in Fig. 5, where the quark momenta have been extended up to high values.

In Fig. 8, we show the creation probability of mesons as a function of temperature. This figure was taken from a calculation with an initial radius of 6 fm and a momentum distribution without cutoff, but the result does not strongly vary for different initial conditions, except for statistical fluctuations. The solid curve, which denotes the pion creation probability, shows the same behavior as for a two flavor plasma [13]. The pion production takes place at a temperature well below the pion Mott temperature, within a temperature range of roughly $150 \text{ MeV} < T < 200 \text{ MeV}$. The same is true for kaons and η mesons, for which the creation probability does not show a significant deviation of the pion creation probability. The qualitative behaviour of these curves can be understood by considering the mean hadronization time of quarks, which for thermal equilibrium has been displayed in Fig. 23 of Ref. [16]. It has been shown there that this quantity has a minimum for $150 \text{ MeV} < T < 200 \text{ MeV}$, thus leading to a minimum of the mean free path, so that one observes a maximum of hadronization processes in this range. A qualitatively similar curve as in Fig. 8 has been obtained in Ref. [13], where, however, only the pion case was considered.

The mean production temperatures according to Fig. 8 amount to 168 MeV for pions, 164 MeV for kaons and 178 MeV for η mesons. These almost identical numbers have to be compared with the Mott temperature, at which in an equilibrated, adiabatically expanding system the hadronization takes place. Due to the finite mean free path, the temperature in our calculations drops well below the Mott temperature before the hadronization can take place.

C. Expansion Dynamics

In Fig. 9, we show the root mean square distances of the individual particle species from the centre for a system with initial conditions as in Tab. I and initial radius 7 fm. As can be seen, the root mean square radius is largest for pions, followed by light quarks, kaons, strange quarks and η mesons. Thus the mesons separate in coordinate space during their expansion, which has consequences for the rescattering models on the hadronic level, as employed by standard cascade calculations. The

same picture can be found in Tab. IV, where we give the mean energy, momentum and velocity for each particle species in the final state. Again one finds the largest velocity for pions, followed by light quarks, kaons, η mesons and strange quarks. This order is roughly an ordering by the particle masses and can be explained partially by the production mechanisms of the particles. If one considers e.g. pions, then one has to take into account that pions are mainly produced via the annihilation of light quark-antiquark pairs. For this process, the rest mass of the final state is usually lower than the rest mass of the initial state, so that the momenta of the pions have to be higher than those of the quarks, which in turn leads to a higher velocity. The same is true if a kaon pair is generated from a strange-antistrange pair. During the expansion, quarks are slowed down by the mean field, whereas mesons become accelerated. This leads to a even higher momentum difference between quarks and mesons. However, strange quarks are not so strongly slowed down as light quarks, since their mass is already high in the initial state. Although the above argument should be also true for strange quarks, which are created from light quarks, we find thus a slightly higher momentum for strange quarks as compared to light quarks.

Table IV shows that the complicated dynamics of the expansion of the $SU(3)$ plasma creates an asymptotic momentum of the kaons and pions which is for our initial condition close to experiment at midrapidity [20]. We see as well that the mean momentum of kaons is larger than the one of pions. This effect, which has also been observed by experiment, has been interpreted as a consequence of rescattering of the mesons [21]. We see here that this increase is not necessarily a hadronic effect, but may already be created during the expansion of the plasma phase, if there is one. The meson momenta are always larger than the momenta of the collision partners which have produced them. This again reflects the fact that at the moment of their creation the temperature is below the Mott temperature and therefore the mass of the $q\bar{q}$ pair is considerably higher than that of the two produced mesons.

IV. SUMMARY AND CONCLUSIONS

In this paper we have studied the expansion and hadronization of a quark-meson plasma using an effective chiral interaction. We have concentrated on aspects of the evolution which are specific to the $SU(3)$ case. Other topics, which can be treated in

the two flavor case as well as in the three flavor case have been discussed in Ref. [13].

We find that the strange quark mass is considerably larger than the current strange quark mass and that it gets even enhanced by initial conditions not containing strange quarks. This has consequences for the production dynamics, since the threshold for the creation of a strange quark pair rises. We find that it is difficult to produce the experimentally observed ratio of strange particles to all particles unless we assume the presence of strange quarks in the initial state. In any case our findings question the assumption of thermal free gas models, in which quarks are treated as particles with their bare mass, or hydrodynamical calculations, which use an equation of state which is based on this assumption.

Concerning the expansion dynamics, we find that the different particle species become separated in coordinate as well as in momentum space. Partially this can be understood by the production mechanisms, as e.g. the relation between light quark and pion momenta, for other species one has concurring effects, so that there is no simple explanation. Using an initial density of $1\text{--}2\text{ GeV/fm}^3$, which has been proposed for the phase prior to the expansion in a plasma created at SPS energies, we find that the average momenta of pions and kaons observed in our calculations are roughly consistent with experimental data. These two effects cannot be modeled in hydrodynamical calculations as well.

The heavy ion experiments performed at CERN do not show a baryon free ($\mu = 0$) midrapidity region. To understand these reactions in detail, the expansion of a plasma at finite baryochemical potential has to be studied. This is presently under way.

REFERENCES

- [1] P. Koch, B. Müller and J. Rafelsky, Phys. Rep. **142**, 167 (1986).
- [2] Y. Nambu and G. Jona-Lasinio, Phys. Rev. **122**, 345 (1961); Y. Nambu and G. Jona-Lasinio, Phys. Rev. **124**, 246 (1961).
- [3] S.P. Klevansky, Rev. Mod. Phys. **64**, 649 (1992); T. Hatsuda and T. Kunihiro, Phys. Rep. **247**, 221 (1994).
- [4] Chr. V. Christov, A. Blotz, H. C. Kim, P. Pobylitsa, T. Watabe, T. Meissner, E. Ruiz Arriola and K. Goeke, Prog. Part. Nucl. Phys. **37**, 91 (1996).
- [5] E. Quack, P. Zhuang, Yu. Kalinovsky, S.P. Klevansky and J. Hüfner, Phys. Lett. B **348**, 1 (1995).
- [6] J. Hüfner, S.P. Klevansky and P. Rehberg, Nucl. Phys. A **606**, 260 (1996).
- [7] E. Laermann, Nucl. Phys. A **610**, 1c (1996); E. Laermann, Nucl. Phys. B (Proc. Suppl.) **60A**, 180 (1998).
- [8] W.-M. Zhang and L. Wilets, Phys. Rev. C **45**, 1900 (1992); W. Florkowski, J. Hüfner, S.P. Klevansky and L. Neise, Ann. Phys. (NY) **245**, 445 (1995); S.P. Klevansky, A. Ogura and J. Hüfner, Ann. Phys. (NY) **261**, 37 (1997).
- [9] P. Rehberg and J. Hüfner, Nucl. Phys. A **635**, 511 (1998).
- [10] P. Rehberg, Phys. Rev. C **57**, 3299 (1998).
- [11] A. Abada and J. Aichelin, Phys. Rev. Lett. **74**, 3130 (1995).
- [12] L. Bot and J. Aichelin, J. Phys. G **23**, 1947 (1997).
- [13] P. Rehberg, L. Bot and J. Aichelin, *Expansion and Hadronization of a Chirally Symmetric Quark-Meson Plasma*, Subatech Preprint SUBATECH-98-16, hep-ph/9809565 (1998).
- [14] J. Aichelin, Phys. Rep. **202**, 233 (1991); Ch. Hartnack, R. K. Puri, J. Aichelin, J. Konopka, S. A. Bass, H. Stöcker, W. Greiner, Euro. Phys. J. **1**, 151 (1998).
- [15] E. Quack and S.P. Klevansky, Phys. Rev C **49**, 3283 (1994); J. Müller and

- S. P. Klevansky, Phys. Rev. C **50**, 410 (1994); V. Dmitrašinović, H.-J. Schulze, R. Tegen and R. H. Lemmer, Ann. Phys. (NY) **238**, 332 (1995).
- [16] P. Rehberg, S. P. Klevansky and J. Hüfner, Phys. Rev. C **53**, 410 (1996).
- [17] P. Zhuang, J. Hüfner, S. P. Klevansky and L. Neise, Phys. Rev. D **51**, 3728 (1995); P. Rehberg, S. P. Klevansky and J. Hüfner, Nucl. Phys. A **608**, 356 (1996).
- [18] J. Hüfner, S. P. Klevansky, E. Quack and P. Zhuang, Phys. Lett. B **337**, 30 (1994).
- [19] M. Gaździcky and D. Röhrich, Z. Phys. C **71**, 55 (1996).
- [20] I. G. Bearden et al., Phys. Rev. Lett. **78**, 2080 (1997).
- [21] H. van Hecke, H. Sorge, N. Xu, *Evidence of Early Multistrange Hadron Freezeout in High Energy Nuclear Collisions*, nucl-th/9804035 (1998); S. Bass et al., Prog. Part. Nucl. Phys. **41**, 225 (1998).

TABLES

r_0 (fm)	N_q	N_s	N_π	N_K	N_η
3	144	0	81	2	1
4	303	1	215	1	10
5	541	5	477	5	20
6	881	5	879	7	40
7	1310	14	1497	18	57

TABLE I. Particle Multiplicities in the final state. The numbers are summed over all internal degrees of freedom, such as flavor, particle/antiparticle and isospin. No strange particles are present in the initial state.

r_0 (fm)	N_q	N_s	N_π	N_K	N_η
3	399	21	224	37	27
4	897	61	560	117	41
5	1304	101	1185	171	118
6	2939	203	2186	291	154

TABLE II. Particle Multiplicities in the final state for initial conditions without momentum cutoff. The numbers are summed over all internal degrees of freedom, such as flavor, particle/antiparticle and isospin. No strange particles are present in the initial state.

r_0 (fm)	N_q	N_s	N_π	N_K	N_η
3	118	36	117	30	3
4	303	87	244	71	11
5	557	147	539	143	16
6	862	234	1076	248	27

TABLE III. Particle Multiplicities in the final state for initial conditions with strange quarks in the initial state. The momentum cutoff has been allied to the initial conditions. The numbers are summed over all internal degrees of freedom, such as flavor, particle/antiparticle and isospin.

	$\langle E \rangle$ (MeV)	m (MeV)	p (MeV)	v
q	525	368	374	0.713
s	676	550	393	0.581
π	441	135	420	0.952
K	698	497	490	0.702
η	674	515	435	0.645

TABLE IV. Mean particle energies, masses, momenta and velocities in the final state. The initial conditions are the same as in Table I, the initial radius is 7 fm.

FIGURES

FIG. 1. Constituent quark masses at finite temperature in equilibrium. Solid line: light quarks, dashed line: strange quarks.

FIG. 2. Feynman graph for the irreducible pseudoscalar polarization. Solid lines denote constituent quarks.

FIG. 3. Meson masses as a function of temperature. Also shown are $2m_q$ and $m_q + m_s$. The Mott transitions of the pion, the kaon and the eta are marked by the arrows.

FIG. 4. Constituent quark masses averaged over all solid angles as a function of r for different times. The lower line is for light quarks, the upper line for strange quarks, respectively.

FIG. 5. Time evolution of the particle multiplicities with initial condition corresponding to Table II. Solid line: light quarks, dashed line: strange quarks, dotted line: pions, dot-dashed line: kaons, double dashed line: η mesons.

FIG. 6. Time evolution of the angular averaged particle density with initial condition corresponding to Table II. Solid line: light quarks, dashed line: strange quarks, dotted line: pions, dot-dashed line: kaons, double dashed line: η mesons. Please note the different scales at the vertical axes.

FIG. 7. Time evolution of the particle multiplicities with initial condition corresponding to Table III. Solid line: light quarks, dashed line: strange quarks, dotted line: pions, dot-dashed line: kaons, double dashed line: η mesons.

FIG. 8. Creation probability of mesons as a function of temperature. Solid line: pions, dashed line: kaons, dotted line: η mesons. The pion Mott temperature is indicated by the vertical line.

FIG. 9. Root mean square radius for each particle species as a function of time. Solid line: light quarks, dashed line: strange quarks, dotted line: pions, dot-dashed line: kaons, double dashed line: η mesons.

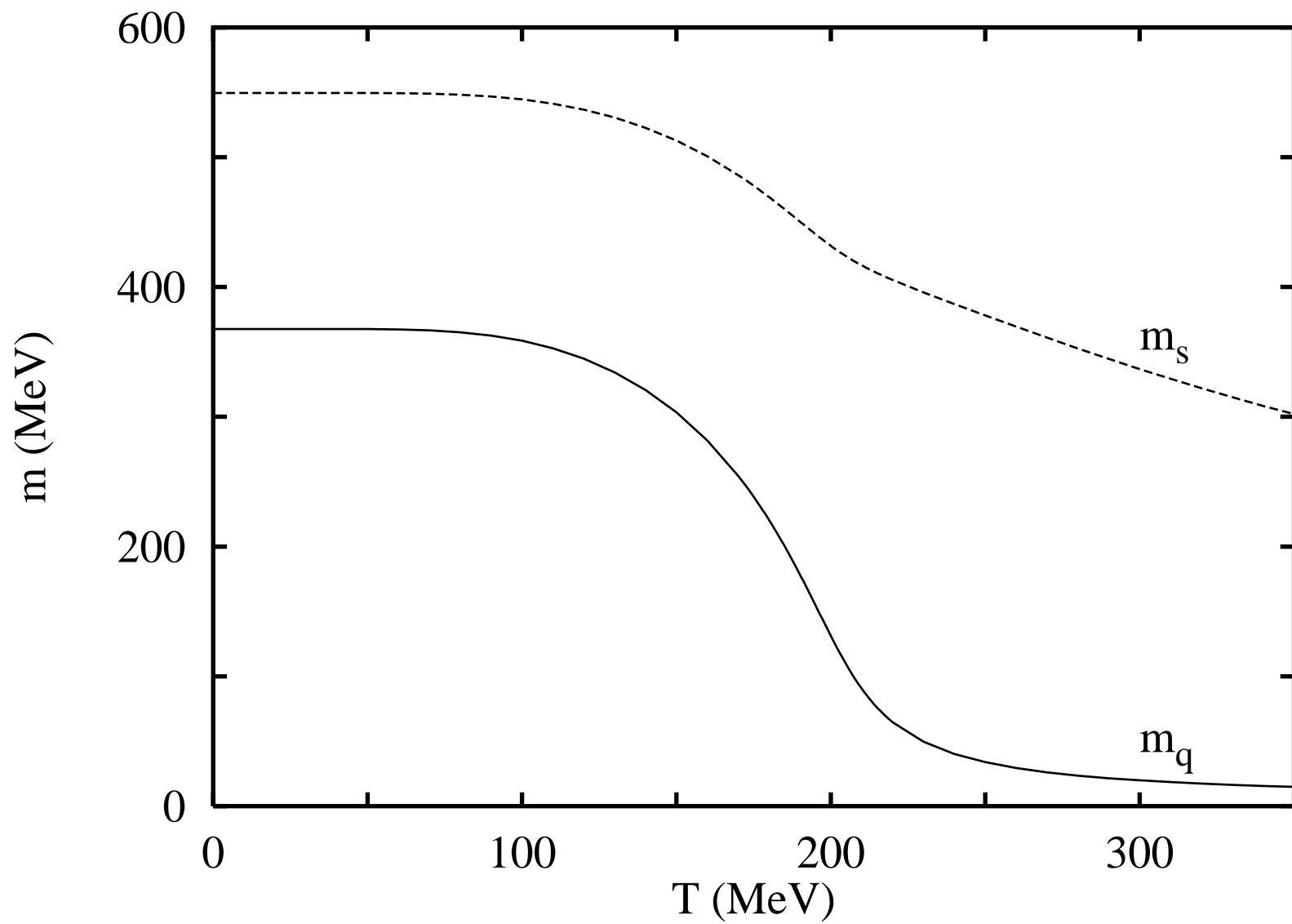


Figure 1

$$-i\Pi_{PS} = \bullet \begin{array}{c} \xrightarrow{i\gamma^5\lambda} \\ \xleftarrow{i\gamma^5\lambda^\dagger} \end{array} \bullet$$

Figure 2

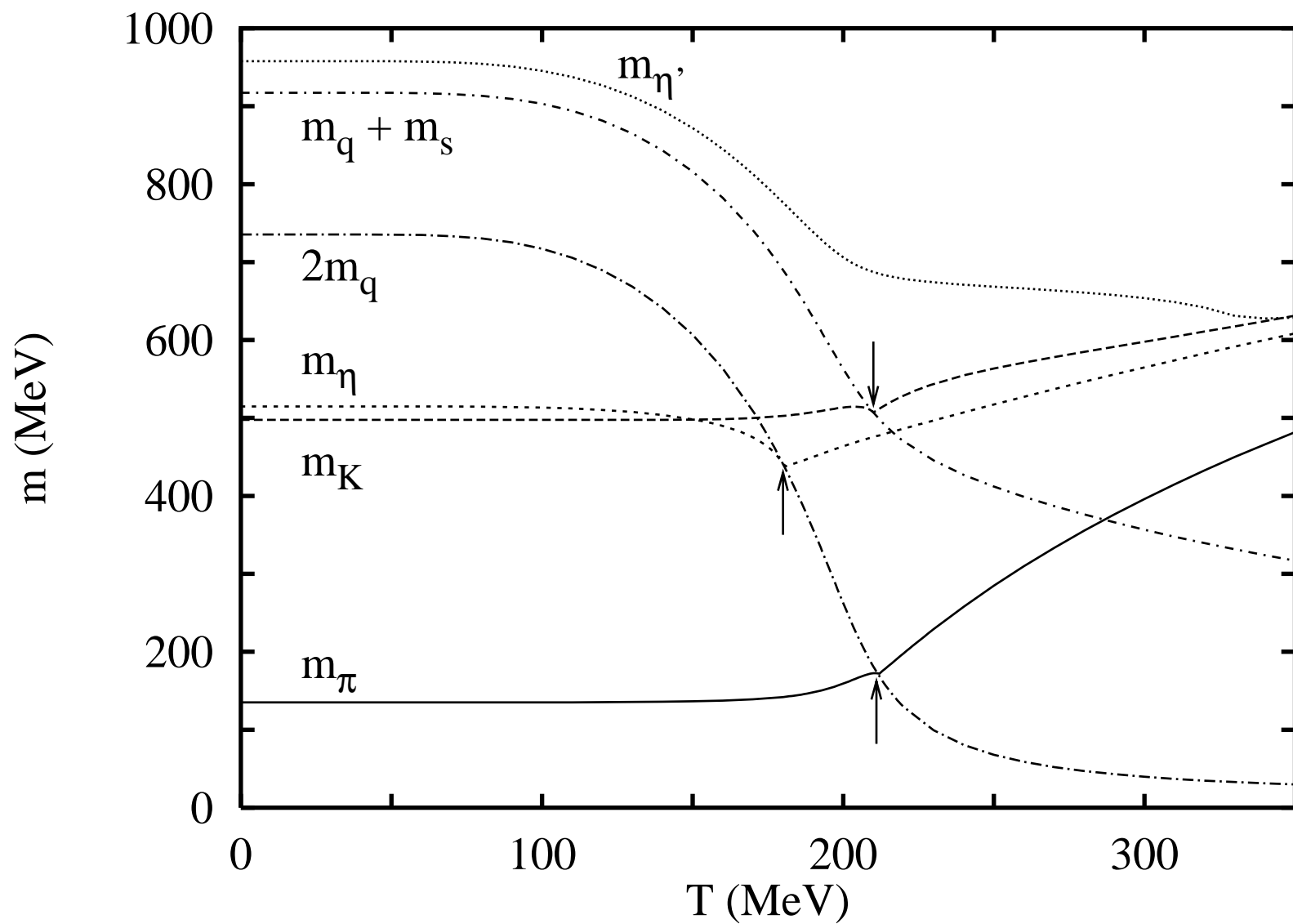
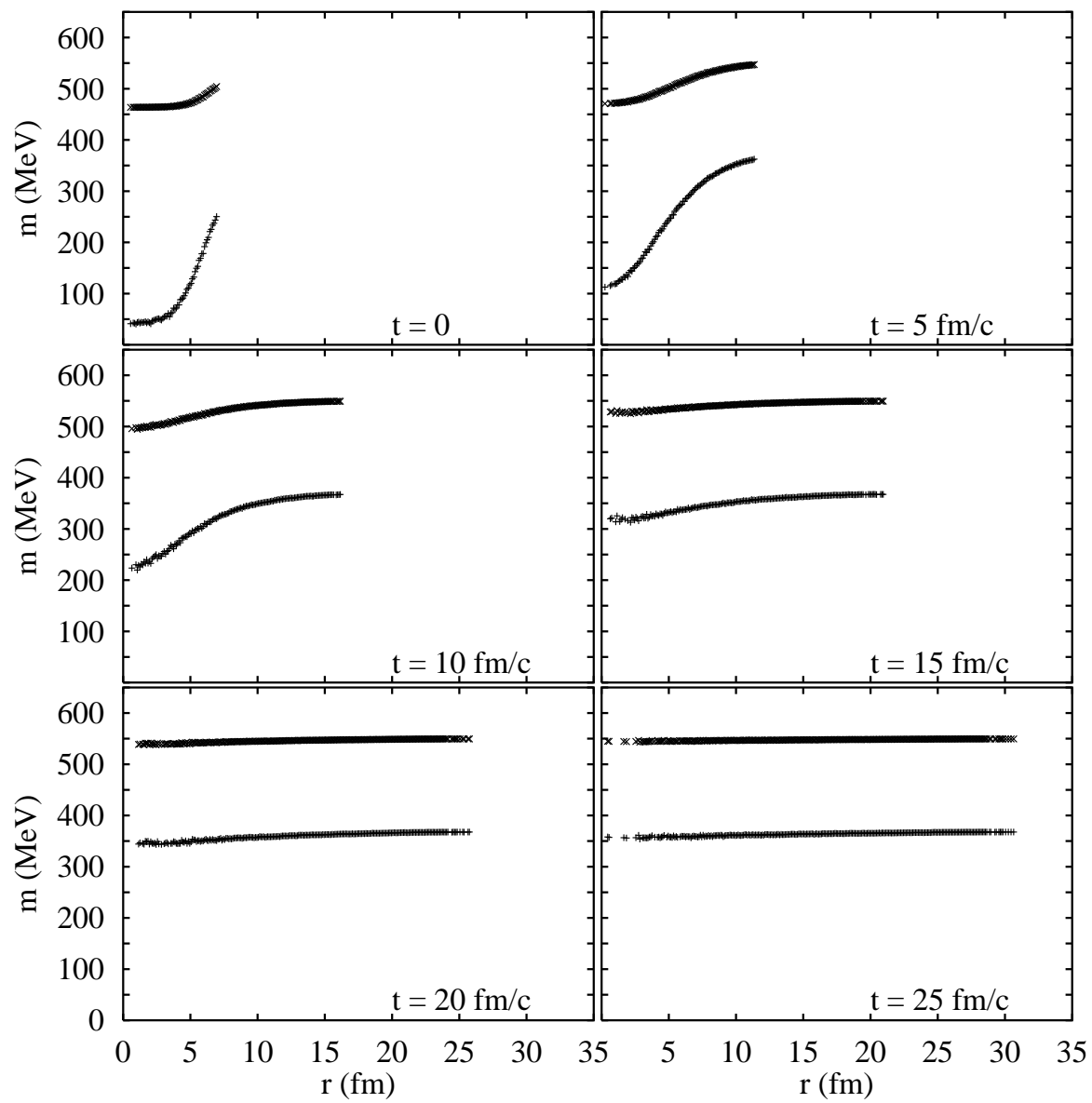


Figure 3

Figure 4



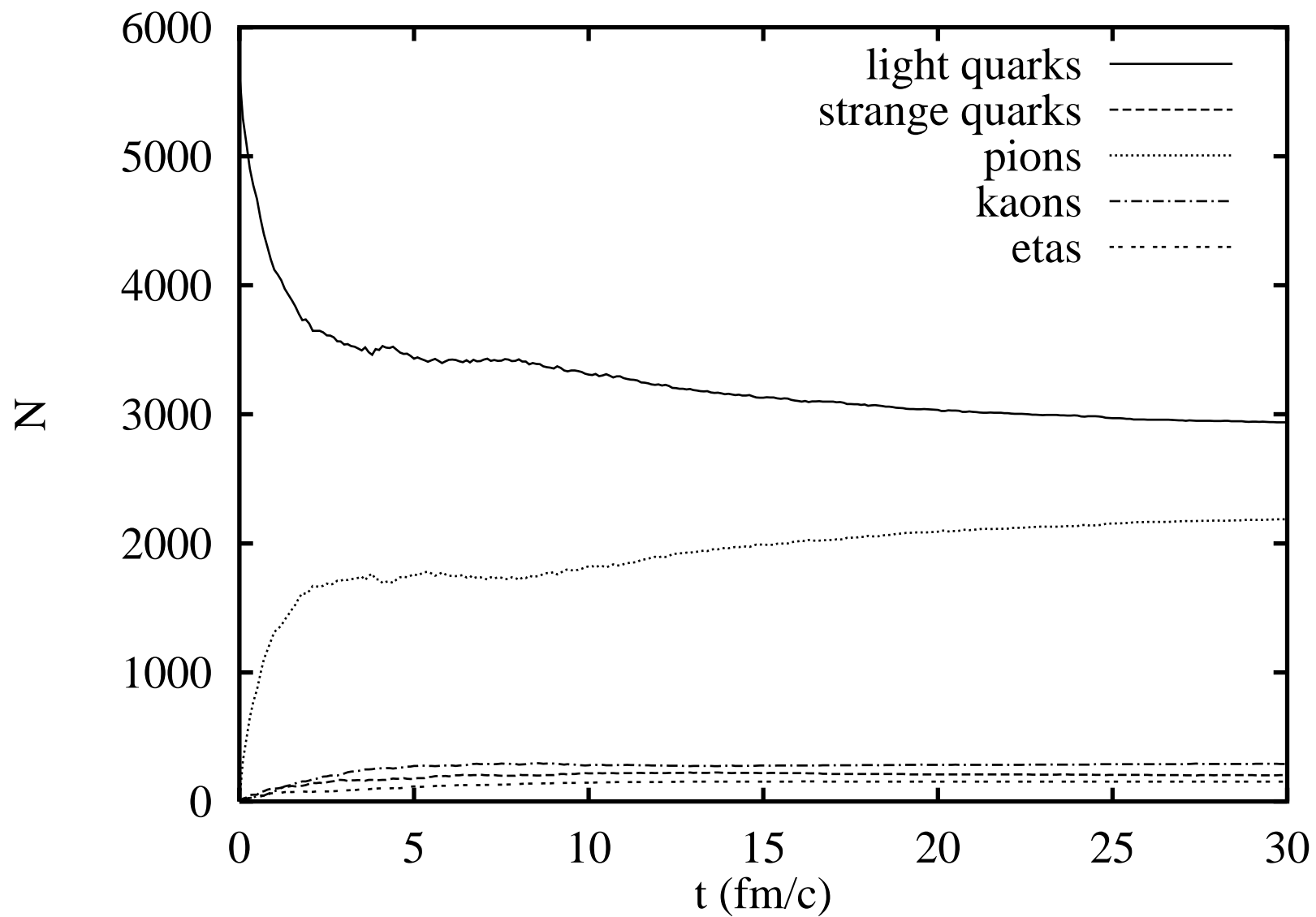
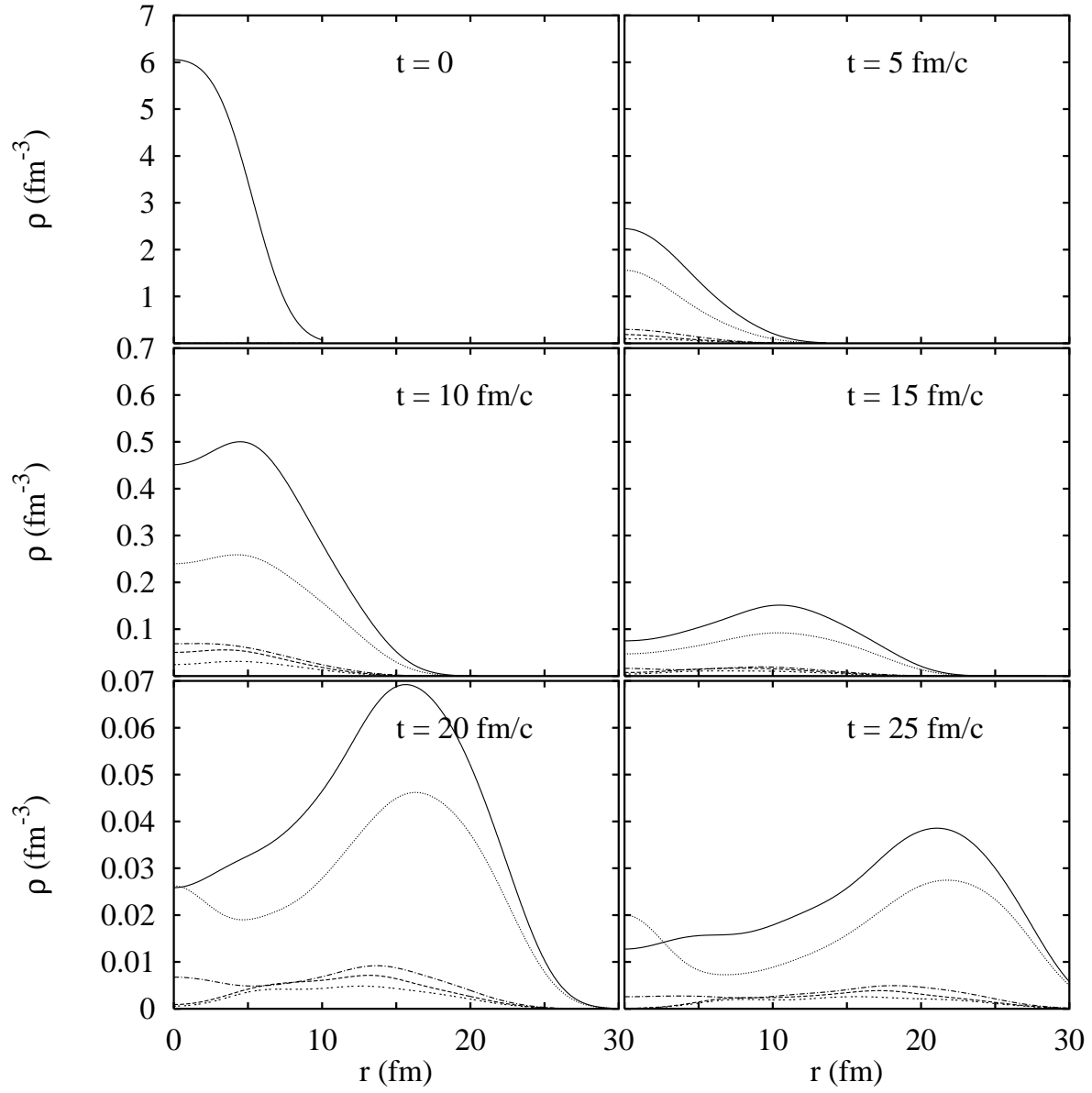


Figure 5

Figure 6



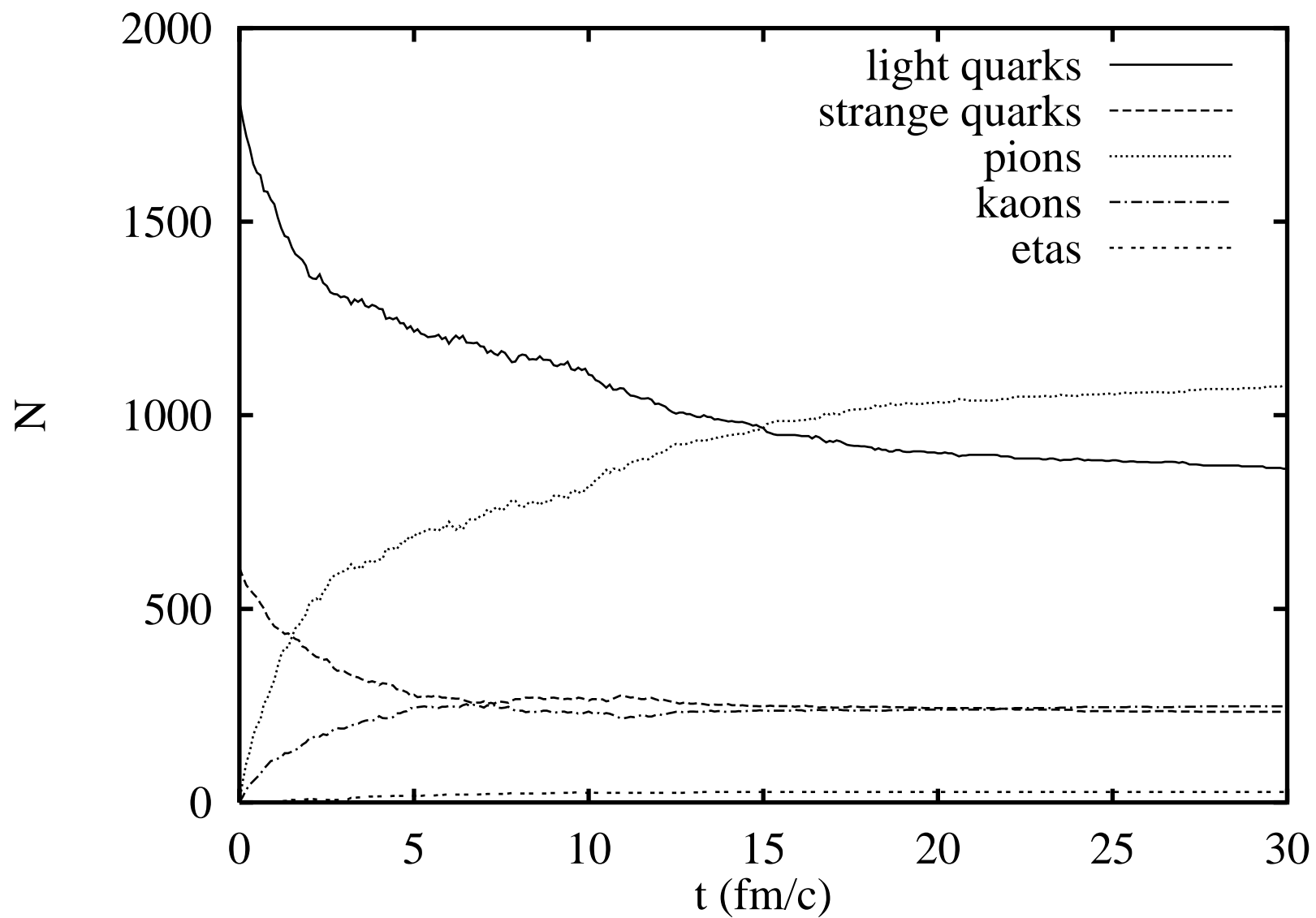


Figure 7

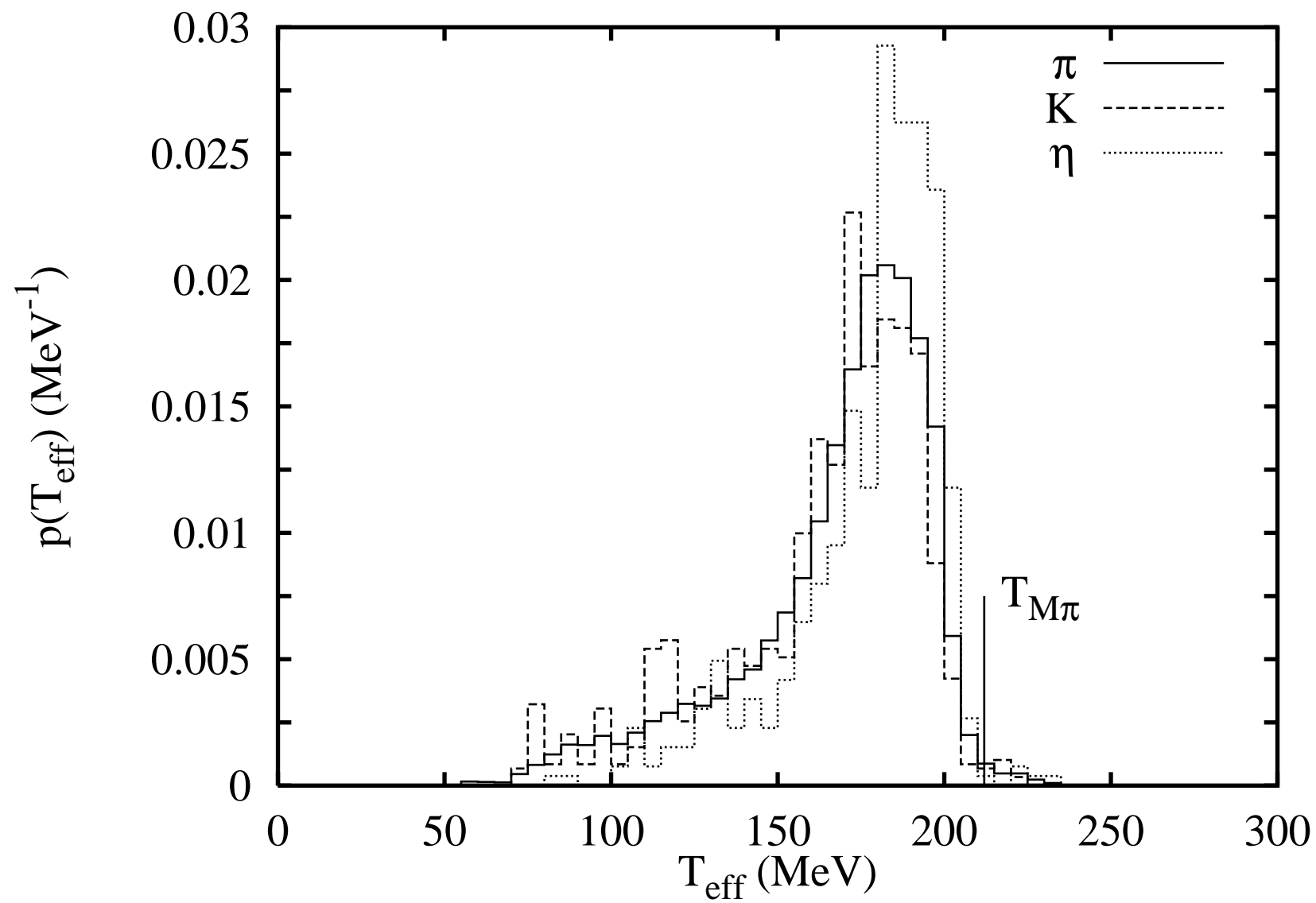


Figure 8

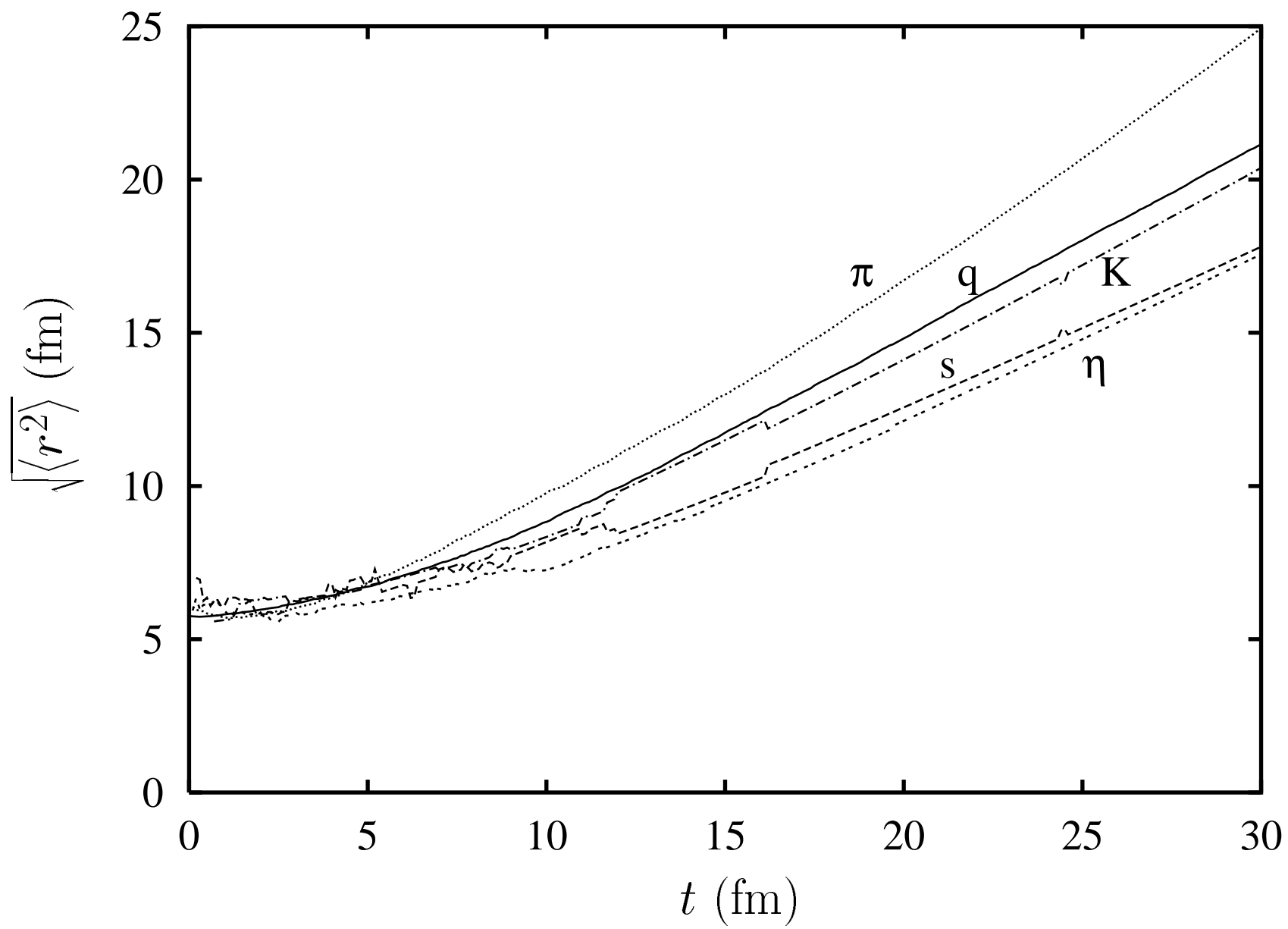


Figure 9